Advances in Water Resources 57 (2013) 32–40

Contents lists available at SciVerse ScienceDirect

Advances in Water Resources

journal homepage: www.elsevier.com/locate/advwatres

Anomalous trend in soil evaporation in a semi-arid, snow-dominated watershed

Rui Wang [a], Mukesh Kumar [a,*], Danny Marks [b]

[a] Nicholas School of Environment, Duke University, Durham, NC 27708, USA
[b] USDA Agricultural Research Service, Northwest Watershed Research Center, Boise, ID 83712, USA

ARTICLE INFO

Article history:
Received 27 July 2012
Received in revised form 16 December 2012
Accepted 13 March 2013
Available online 28 March 2013

Keywords:
PIHM
ISNOBAL
Coupling
Snow covered area (SCA)
Modeling

ABSTRACT

Soil evaporation in arid and semi-arid regions is generally moisture-limited. Evaporation in these regions is expected to increase monotonically with increase in precipitation. In contrast, model simulations in a snow-dominated, semi-arid Reynolds Mountain East (RME) watershed point to the existence of an anomalous trend in soil evaporation. Results indicate that soil evaporation in snow-dominated watersheds first increases and then subsequently decreases with increasing precipitation. The anomalous variation is because of two competing evaporation controls: (a) higher soil moisture in wetter years which leads to larger evaporation, and (b) prolonged snow cover period in wetter years which shields the soil from the atmosphere, thus reducing soil evaporation. To further evaluate how the competition is mediated by meteorological and hydrogeological characteristics of the watershed, changes in the trend due to different watershed hydraulic conductivity, vegetation cover, and snowfall area fraction are systematically studied. Results show considerable persistence in the anomalous trend over a wide range of controls. The controlling factors, however, have significant influence both on the magnitude of the WY evaporation and the location of the inflection point in the trend curve.

© 2013 Elsevier Ltd. All rights reserved.

1. Introduction

Evapotranspiration (ET) is one of the primary hydrologic exchange fluxes between the terrestrial and atmospheric continuum that determines the partitioning of precipitation in different water stores thus influencing the overall response of the watershed. The importance of ET on hydrology and ecology has been widely studied.

ET loss from a watershed, and its temporal and spatial variability, depends on a variety of watershed properties and climate forcings such as precipitation, air temperature, relative humidity, net radiation, vapor pressure, vegetation and soil moisture retention etc. [1]. Overall, variation in ET is determined by the balance between available energy and soil moisture [2,3]. Investigation of evaporation data from 1200 moderate sized catchments with climate regimes ranging from arid to wet humid settings showed that regional evaporation is limited by water availability in environments, while it is energy limited in humid environments [4]. Subsequent studies [2,5] also confirmed the view that in rain-dominated watersheds, ET in arid or semi-arid regions is proportional to precipitation while ET in humid regions is proportional to available energy.

In recent decades, climate warming-induced severe drought and water shortage problems in snow-dominated regions have drawn wide attention [6–9]. ET in these regions makes up a large proportion of water budget [3,10–12], and has been highlighted as an area with substantial need for more research and understanding [3,13]. While studies regarding ET in snow-dominated watersheds have generally focused on the role of ET in water budget components [3,11,12,14–20], studies concerning the behavior of ET particularly in relation to total precipitation in snow-dominated watersheds is limited.

Analysis of 25 water years (WY)[1] of long term observed precipitation and discharge from the Reynolds Mountain East (RME) watershed [21], a semi-arid, snow-dominated watershed in the Owyhee Mountains of southwestern Idaho, shows an inverse relationship, or conservatively stated, a non-increasing relationship between WY precipitation and the sum of ET and Net storage (Fig. 1). If the net WY storage in the watershed shows a non-decreasing variation with increasing WY precipitation, Fig. 1 can be used to imply that ET loss also has an inverse relationship to the amount of WY precipitation. Observed change in groundwater depths (Fig. 1) indicate that the watershed experiences a net gain in WY storage for the years receiving larger precipitation. This means that a stronger

* Corresponding author.
E-mail address: mukesh.kumar@duke.edu (M. Kumar).

[1] A water year runs from October through September. The water year is used in the western USA because most precipitation falls during the winter and spring months of November through April.

0309-1708/$ - see front matter © 2013 Elsevier Ltd. All rights reserved.
http://dx.doi.org/10.1016/j.advwatres.2013.03.004

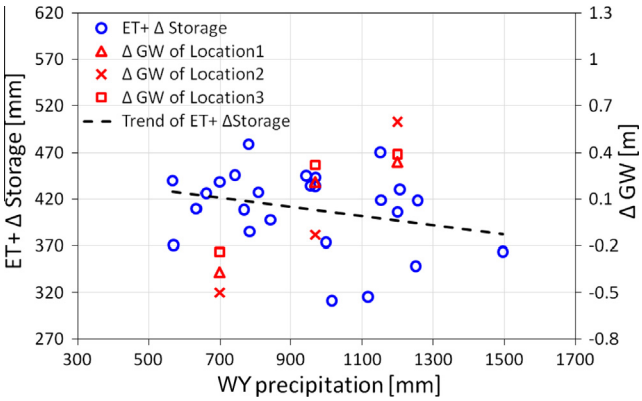

Fig. 1. WY ET + ΔStorage (equals WY precipitation minus WY runoff) versus WY precipitation based on 25 WYs (1984–2008) of observed data from RME watershed in Idaho. Also shown are ΔGW (WY change in groundwater depth) for three locations during 2006, 2007 and 2008 WYs.

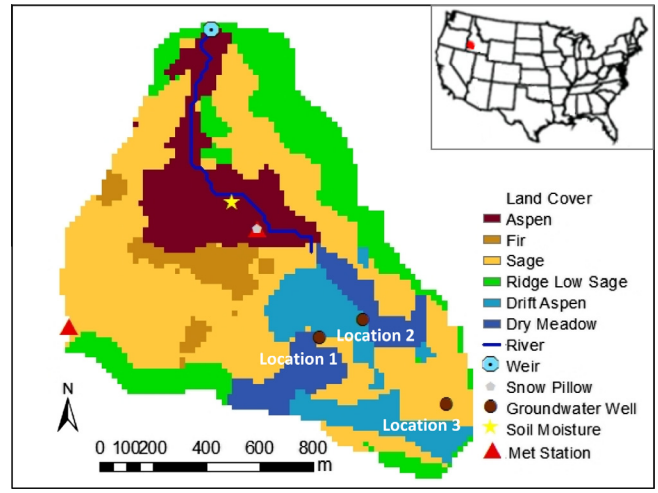

Fig. 2. Land cover and locations of stream gage, snow pillow, groundwater well, soil moisture and meteorological stations in the RME watershed.

inverse relationship (than the one shown in Fig. 1) between ET and WY precipitation can be expected in RME watershed. Similar trends were also observed at higher elevations in the Merced River basin of the Sierra Nevada, California. While ET at lower elevations in the Merced River basin showed increases in WY ET with increases in WY precipitation, at higher elevations the WY ET initially increases but subsequently decreases [3]. Notably, the decreasing trend of ET in RME and Merced River basin is antithetical to the established view of hydrology in semi-arid settings where an increased availability of moisture from precipitation is expected to result in larger evaporation. The reasons for the existence of this anomalous trend, and how it may be influenced by meteorological forcings such as the magnitude of precipitation and temperature, and watershed properties such as vegetation cover and effective watershed conductivity is largely unclear.

This paper explores the relationship between only the soil evaporation component of ET and the WY precipitation, and evaluates how the relationship will be affected by watershed properties, land cover and snow cover area through four virtual experiments in RME. Using the linked snow model (ISNOBAL) and distributed hydrologic model (PIHM), four virtual experiments each with nine precipitation scenarios with increasing magnitudes of water year precipitation are conducted to specifically answer the following four questions: (1) How does soil evaporation change with precipitation magnitude in a snow-dominated semi-arid setting? (2) How is the relation between soil evaporation and precipitation influenced by the equivalent hydraulic conductivity of the watershed? (3) How is variation of watershed average soil evaporation with precipitation influenced by the relative areal cover of shrubs and trees within the watershed? and (4) How does the area fraction of snowfall in a watershed influence the variation of soil evaporation with precipitation? Questions 2, 3 and 4 explore how the trend of soil evaporation is mediated by meteorological and hydrogeological characteristics of snow dominated watersheds. Answers to these questions would help us in understanding the prevalence of this anomalous relationship between precipitation and evaporation in other snow-dominated, semi-arid watersheds.

2. Data and methods

2.1. Study area and data

In order to obtain an integrated understanding of the relationship between evaporation and WY precipitation, we consider the Reynolds Mountain East (RME) watershed (Fig. 2), a field laboratory operated by the USDA Agricultural Research Service in the Owyhee Mountains of southwestern Idaho, for analysis. GIS watershed descriptors and an hourly data set including meteorological forcing and validation data for the water years 1984–2008 for RME are available from Northwest Watershed Research Center, USDA, USA, via anonymous ftp (ftp://ftp.nwrc.ars.usda.gov/public/RME_25yr_database) [21]. The RME watershed is 0.39 km^2 in area and the elevation within the watershed ranges from 2027 m to 2137 m. About 30% of the RME catchment is forested with the remainder of the basin consisting of dry meadow and mixed sagebrush. Twenty-five year (1984–2008) basin average water year precipitation and outflow from the RME watershed are 964 and 505 mm, respectively [21]. The watershed received 70% of its precipitation in the form of snow.

2.2. The linked ISNOBAL and PIHM model

Here we link the 2 layer energy- and mass-balance snowmelt model-ISNOBAL [22–24] and the integrated distributed hydrologic model-PIHM [25–27] to simulate the snowmelt and hydrological process of the watershed. ISNOBAL solves the snow cover energy- and mass-balance at each grid cell in a digital elevation model. The model uses a two-layer representation of the snowpack and can be applied to regions with limited data on meteorology, snow structure and temperature. It calculates the energy state, mass balance, melt or refreezing, and liquid water drainage from the snowpack. Temperature and snow water equivalent for each layer is also simulated. Melt is computed in either layer when the layer temperature reaches the melting point (0 °C) and more energy is added. Water drains from the base of the snowpack when the accumulated melt and liquid water content exceed a specified threshold. The model readjusts the snow's mass, thickness, thermal properties and measurement heights for both layers after each time-step. More information regarding the theory, input, and output parameters of the model are presented in [23,24]. PIHM uses a semi-discrete, finite-volume approach to define the distributed process equations on discretized unit elements. It simulates five hydrologic states (snow water equivalent, soil moisture of the surface layer, unsaturated zone soil moisture, groundwater depth and stream stage), at each discretization unit in the watershed. Physical process representation for streamflow in the model is based on a depth-averaged 1-D diffusive wave equation, surface flow is based on a depth-averaged 2-D diffusive wave approximation of the Saint Venant equations while subsurface flow simulation is based on the

depth-averaged, moving boundary approximation of variably saturated form of Richards's equation [26]. Full coupling between overland and vadose zone flow is based on the continuity of head and flux. An integrated GIS framework, PIHMgis [28] is used to facilitate automated generation of model input files from geodatabases.

For this study, ISNOBAL and PIHM are linked using a one-way coupling strategy. The linked model has been previously used [17] to explore and compare the influence of snow accumulation, redistribution and melt on variations in surface and subsurface hydrologic states and mass fluxes in different land covers, for a wet and dry year. Linkage involves deactivation of the temperature index snowmelt utility in PIHM, and instead using the snowmelt output from ISNOBAL as a flux boundary condition on the PIHM kernel. In addition, soil evaporation in PIHM is shut off at locations shielded by accumulated snow. Energy exchanges at snow-free locations remain the same. Soil evaporation at a point is calculated as follows:

$$E_{s,t} = S_{s,t} \cdot E_{p,t} \cdot \delta_t \tag{1}$$

$$\delta_t = \begin{cases} 0 & Z_{s,t} > 20\,\text{mm} \\ 1 & Z_{s,t} \leqslant 20\,\text{mm} \end{cases} \tag{2}$$

where $E_{s,t}$ is actual soil evaporation at time t (mm/h); $S_{s,t}$ is soil saturation of the top soil layer at time t; $E_{p,t}$ is potential evapotranspiration at time t (mm/h); $Z_{s,t}$ is snow depth at time t (mm); δ_t is a shielding factor that is set equal to zero for snow cover depths beyond a threshold. So for snow cover depths larger than the threshold (=20 mm), soil evaporation is set equal to zero because of shielding. At this grid-averaged snow depth, mass and energy exchange takes place at snow-air and snow-ground interface rather than at ground-air interface. Potential evaporation $E_{p,t}$ (mm/d) is calculated based on Penman Equation [29,30]:

$$E_{p,t} = \frac{(R_n - G)\Delta + \left(\frac{\rho C_{pa}}{r_a}\right)(e_s - e_a)}{\Delta + \gamma} \tag{3}$$

where R_n is net radiation at the vegetation surface (MJ/m^2/d), G is soil heat flux density (MJ/m^2/d), C_{pa} is specific heat capacity of air, r_a is atmospheric diffusive resistance, $e_s - e_a$ is saturation vapor pressure deficit (kPa), Δ is the slope of the vapor pressure curve (kPa/°C), and γ is the psychrometric constant (kPa/°C). Evaporation from the whole watershed is sum of $E_{s,t}$ calculated within each discretization cells.

2.3. Model calibration and application

ISNOBAL needs no calibration. Calibration of the hydrology model is performed independently of the melt inputs from snow model. The process involves nudging of hydrogeological parameters uniformly across the model domain, to match the magnitude and rate of the hydrograph decay during recession. Calibration is limited to 2006–2008 water year. More details of the calibration strategy are presented in [17]. In this paper, observed stream flow and hourly climate forcing data such as precipitation, air temperature, net radiation, relative humidity, wind speed and vapor pressure, from 2006 to 2008 water year are used to drive the ISNOBAL and PIHM model. The chosen three year simulation period ensures availability of transient validation data sets and allows validation at seasonal and WY scales, and encompasses meteorologically diverse forcing conditions. 2006 water year was very wet while 2007 water year was dry. WY precipitation for 2008 water year is close to the average WY precipitation during 1984–2008. The linked models simulate snow water equivalent (SWE), snowmelt, sublimation and evaporation, overland flow and ponding, depth-averaged unsaturated soil moisture in the top 25 cm and the unsaturated zone below it, groundwater head and stream stage for each cell. Calibrated hourly hydrologic states, such as SWE at the snow pillow site, streamflow, soil saturation in the top 25 cm and groundwater depth at three other locations are shown in Fig. 3. Details about the ancillary data sets used in the simulation can be referred to in Kumar et al. [17]. The coefficients of determination (*CD*) and the Nash–Sutcliffe efficiency (*NSE*) [31] for simulated results are shown in Table 1. Though the observed groundwater responses at wells 1 and 2 were unusually steep, varying as much as 7.5 m in a matter of three hours, the model was able to adequately capture these dynamics. More detailed characterization of the subsurface, finer data and model grid resolution and an automated calibration strategy may help resolve this problem. It is also probable that the simple representation of macro-porous flow behavior in the model subsurface is not adequate for highly transient subsurface flow systems. Despite using a non-localized calibration approach [17], the model predictions for SWE, streamflow and surface soil moisture are reasonably. In addition, the simulated and observed annual runoff mean during WYs 1984–2008 were 510 mm and 530 mm, respectively. Simulated basin-average ET for WY 2007 was 440 mm, which is approximately the same as the the reported value of 421 mm based on the eddy-covariance flux measurement over shrub (265 mm), aspen and fir (108 mm), and understory (48 mm) [10]. It is to be noted that the validation of evaporative fluxes is performed only to establish some confidence in the model being used, and not to improve the hydrologic characterization of the watershed.

Using the calibrated ISNOBAL–PIHM model, we perform four virtual experiments to answer the questions listed above. All the experiments include nine precipitation scenarios with increasing WY precipitation. Considering precipitation series of 2008 water year (WY precipitation is 996 mm) as the base case, nine precipitation scenarios are generated by rescaling the magnitudes of hourly snowfall ($P_{s,t}$) in 20% $P_{s,t}$ increments. The result is nine precipitation series with WY magnitude ranging from 384 mm to 1608 mm, even while the WY rainfall is kept the same. This allows us to analyze the trend in evaporative loss in relation to the magnitude of WY precipitation due to increase in snowfall. Climate forcings for 2008 water year (WY precipitation = 996 mm), a median precipitation year during 1984–2008, were used as the base case forcings in all the experiments.

3. Results

The results are presented thematically following the four questions outlined in Section 1.

3.1. Evaporation increases and subsequently decreases with increasing precipitation magnitude in snow-dominated semi-arid setting

The linked model is applied to RME watershed to evaluate how the changes in magnitude of precipitation potentially affect the evaporative loss. Two cases are simulated: a "Snow Dominant" case and an "All Rain" case. The "Snow Dominant" case considers WY precipitation time series consisting of both rain and snow events. Nine scenarios (WY precipitation range from 384 mm to 1608 mm) with same amount of WY rain but increasing WY snowfall are used in the "Snow Dominant" case. The "All Rain" case considers the precipitation time series consisting of only rain. Nine precipitation scenarios used in the "All Rain" case are obtained by replacing the snowfall in "Snow Dominant" case with rainfall while all the other climate forcing variables are kept unchanged. The purpose of performing an "All Rain" case simulation is to distinctively evaluate how the trend of evaporation with precipitation is dependent on its phase.

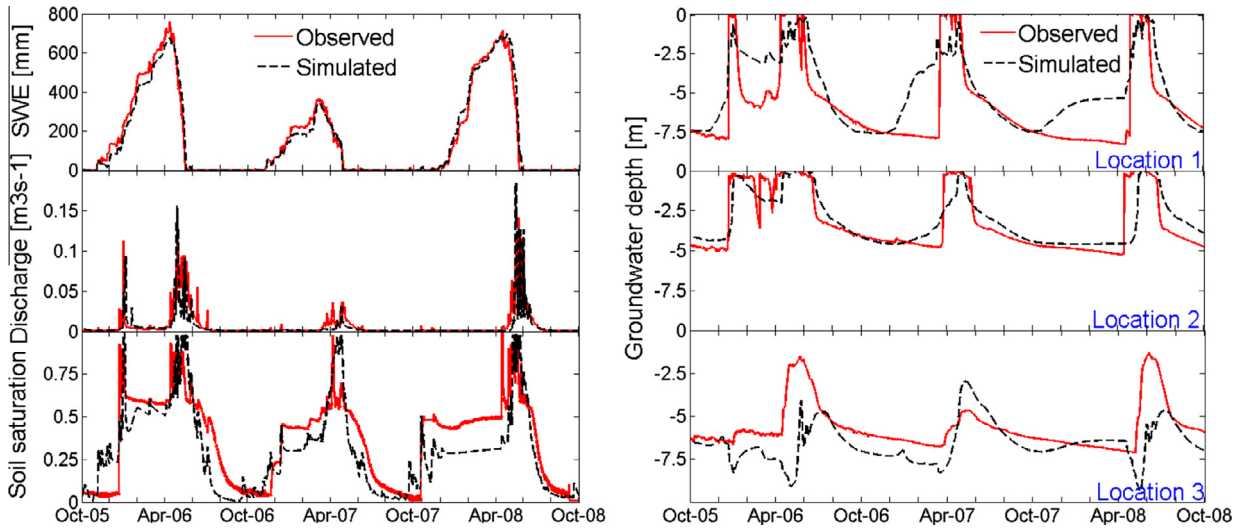

Fig. 3. Observed and simulated hourly snow water equivalent (SWE), discharge of stream, surface soil saturation in top 25 cm and groundwater depth at three different locations in RME watershed from 2006 to 2008 water year.

Table 1
Coefficient of determination (*CD*) and Nash–Sutcliffe efficiency (*NSE*) values of the simulated snow water equivalent (SWE), streamflow, soil moisture and groundwater depth.

	SWE	Streamflow	Soil moisture	Groundwater depth		
				Location 1	Location 2	Location 3
CD	0.98	0.61	0.70	0.58	0.70	0.07
NSE	0.98	0.58	0.61	0.44	0.70	−0.77

Fig. 4 shows the comparison of variation of WY evaporation, transpiration and ET with increasing WY precipitation for the snow and rain-dominated cases. For the same total amount of precipitation, the WY evaporation for the "Snow Dominant" case is smaller than WY evaporation for "All Rain" case (Fig. 4a). Two primary factors for differences between the two cases are timing of water delivery to the soil surface that may participate in soil evaporation, and snow cover that effectively shields the soil surface from atmosphere thus preventing soil evaporation. Snow accumulation delays water delivery to the ground by storing water in the snowpack during the cold season (Dec–Apr). As a result, most of the melt water is delivered in late spring or early summer, the period when net-incoming radiation and air temperature are relatively larger. This would result in WY evaporation in "Snow Dominant" case to be higher than in "All Rain" case. However, accumulated snow in "Snow Dominant" case results in reduction in the area and time for which ground is exposed to atmosphere for evaporation. As a result, the difference of WY evaporation between the two cases increases with the increase of WY precipitation. For the "All Rain" case, the WY evaporation increases monotonically with the increasing amount of precipitation while for the "Snow Dominant" case, the WY evaporation first increases and then subsequently decreases with increasing amount of precipitation (Fig. 4a). The distinctive trend between the two cases points to the fact that the anomalous trend in evaporative loss, in terms of its eventual decrease with increase in precipitation, is a unique characteristic of snowfall dominated precipitation regimes.

In order to explore the reason for anomalous behavior of WY evaporation, evaporation in each month during a year is analyzed. Although WY evaporation initially increased and then subsequently decreased with increasing amount of precipitation for the "Snow Dominant" case, variation of monthly evaporation for the nine scenarios do not exhibit the same trend in different months (Fig. 5a). In late summer and early fall (Jul–Oct), monthly evaporation increases with precipitation. In colder months with extensive snow cover, evaporation is close to zero. And in May–June, evaporation first increases and then decreases with increase in WY precipitation. To identify the reasons behind the

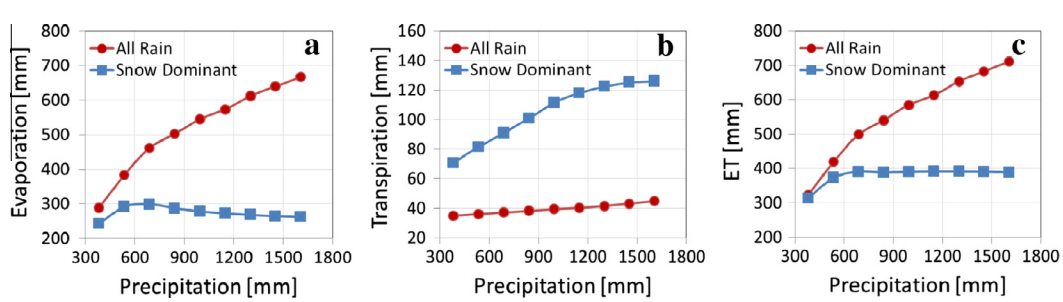

Fig. 4. Simulated WY soil evaporation, transpiration and evapotranspiration (ET) losses for nine precipitation scenarios with WY precipitation ranging from 384 mm to 1608 mm. "All rain" case assumes all the precipitation events to be rain. In "Snow Dominant" case, rain events are kept unchanged and snow events are rescaled to simulate different scenarios. The meteorological conditions are considered to be the same for all cases.

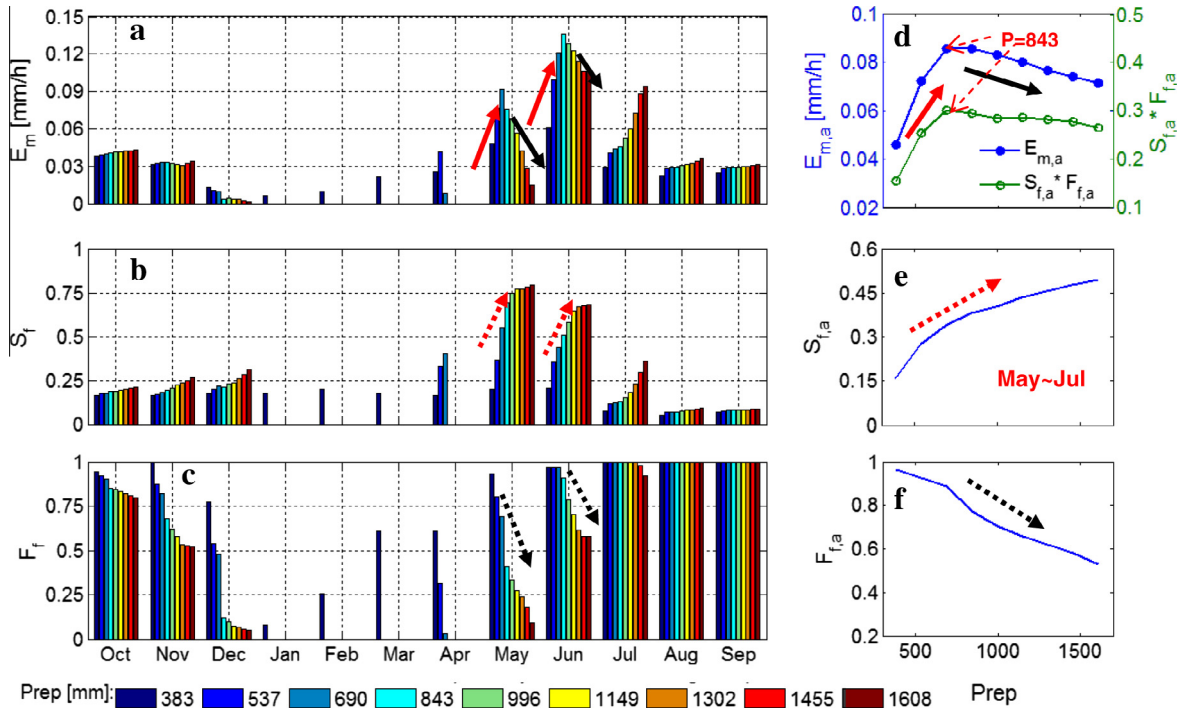

Fig. 5. Watershed averaged monthly soil evaporation (E_m), mean soil saturation in top 25 cm in snow cover-free period for a month (S_f) and the fraction of snow cover-free period over a month (F_f) for the nine precipitation scenarios with different magnitude of WY precipitation (Prep) (Fig. 5a–c). $E_{m,a}$, $S_{f,a}$ and $F_{f,a}$ is the mean E_m, S_f and F_f in May–July (Fig. 5d–f). The upward arrows indicate increases in evaporation (solid arrow) caused by increasing soil moisture (dotted arrow) and the downward arrows indicate decreases in evaporation (solid arrow) caused by decreasing snow cover-free period (dotted arrow).

anomalous trend in WY soil evaporation, variations in monthly soil evaporation for the nine scenarios are analyzed. Monthly soil evaporation, (mm/h), is evaluated using Eq. (1) as:

$$E_m = \frac{1}{M}\sum_{t=1}^{M}(S_{s,t}\cdot E_{p,t}\cdot \delta_t) = \frac{1}{M}\sum_{t=1}^{SFP}(S_{s,t}\cdot E_{p,t}) \tag{4}$$

where M is the total number of hours in a month and SFP is the snow cover free period in a month (hr). Since $E_{p,t}$ is the same between nine precipitation scenarios, differences in the monthly soil evaporation (E_m) are mainly caused by the changes in $S_{s,t}$ and SFP between different scenarios. For qualitative explanation of why the monthly evaporation between nine scenarios is different, Equation (4) is approximated to:

$$E_m \approx \frac{1}{M}\sum_{t=1}^{SFP}(S_{s,t}\cdot E_{p,t}) = S_f\cdot F_f\cdot E_p \tag{5}$$

where E_p and S_f are the mean potential evaporation and soil saturation in snow cover free period for a month, respectively, and F_f is the fraction of snow cover-free period over a month. S_f is indicative of the amount of soil moisture available for evaporation and F_f determines the time for which ground is exposed to the atmosphere for evaporation. Variations in E_m calculated using Eq. (4) for different scenarios are analyzed based on the variations in monthly S_f and F_f (Fig. 5) as presented in Eq. (5). An increasing trend in S_f with increase in precipitation (Fig. 5b) is because of increased snow accumulation in wetter years, which delivers more snow melt to the soil. With more soil moisture available for evaporation, evaporation increases with the increase in snowfall. However, increased WY snowfall also results in a longer period of accumulated snow cover leading to a decreasing trend in F_f (Fig. 5c). Snow cover shields evaporation from the soil surface, thus reducing the evaporation. Hence the variation in evaporation with different amounts of WY precipitation is controlled by the competition between increased evaporation due to increased soil moisture delivery, and reduced evaporation due to longer duration of snow cover. For instance in December, S_f for the nine scenarios is increasing while F_f is decreasing. As the decrease of F_f with increasing amount of precipitation is more significant than the increase of S_f, soil evaporation shows a decreasing trend in December (Fig. 5a–c). On the other hand, in July, the increase of S_f is much more significant than the decrease of F_f, as almost all the snow cover has melted away by then, resulting in an increasing trend in the soil evaporation (Fig. 5a–c). In May and June, the increase of S_f is more significant than the decrease of F_f for smaller precipitation magnitudes. For larger precipitation magnitudes, the rate of increase in S_f is reduced because soil saturation is capped by its maximum value of 1 under wet conditions. This results in a decreasing trend for F_f, which becomes more dominant with increasing precipitation magnitudes. Evaporation in May and June exhibits an increasing trend through moderate precipitation, and then a decreasing trend with further precipitation increases (Fig. 5a–c). Since soil evaporation during May–July accounts for about 60% of average WY evaporation and exhibits significant differences across nine scenarios (Fig. 5a), the anomalous trend in WY evaporation can be qualitatively explained based on the variation in the amount of evaporation during May–July. The mean evaporation during May–July, $E_{m,a}$ (mm/h), can be represented using Eq. (5) as:

$$E_{m,a} \approx S_{f,a}\cdot F_{f,a}\cdot E_{p,a} \tag{6}$$

$$S_{f,a} = \frac{\sum_{i=5}^{7}(S_{f,i}\cdot F_{f,i})}{\sum_{i=5}^{7}(F_{f,i})} \tag{7}$$

$$F_{f,a} = \frac{1}{3}\sum_{i=5}^{7}F_{f,i} \tag{8}$$

$$E_{f,a} = \frac{1}{3}\sum_{i=5}^{7}E_{p,i} \tag{9}$$

where $S_{f,a}$, $F_{f,a}$ and $E_{p,a}$ are the weighted means of $S_{f,i}$, $F_{f,i}$ and $E_{p,i}$, respectively for May, June and July. $S_{f,a}$ and $F_{f,a}$ show an increasing and decreasing trend with increasing precipitation, respectively (Fig. 5e and f). According to Eq. (6), variation in $E_{m,a}$ with increasing precipitation is based on the competition between the rate of increase in $S_{f,a}$ and the rate of decrease in $F_{f,a}$ with increasing precipitation. If the rate of increase in $S_{f,a}$ is larger than the rate of decrease in $F_{f,a}$, $E_{m,a}$ increases, and vice versa. The competition between the two factors is illustrated by the product of $S_{f,a}$ and $F_{f,a}$ (Fig. 5e and f). The curve first increases and then decreases, with the peak coinciding with the trend in $E_{m,a}$. The same trend is also exhibited for WY evaporation. However in the "All Rain" case, no such competition exists. As a result, WY evaporation increases monotonically with increasing WY precipitation.

For the same total amount of precipitation, the WY transpiration for the "Snow Dominant" case is greater than WY transpiration for "All Rain" case (Fig. 4b). This is because snow accumulation causes most of the melt water to be delivered in late spring or early summer when potential transpiration rates are higher, thus allowing plants to optimally use available moisture. It is to be highlighted that WY transpiration keeps on increasing with the increase of WY precipitation in both the "Snow Dominant" and "All Rain" cases. To sum up, for the "Snow Dominant" case, with increasing precipitation, soil evaporation increases and subsequently decreases while transpiration increases monotonically. As a result, ET exhibits a sharp increasing trend followed by a mild decreasing trend with increased WY precipitation (Fig. 4c).

3.2. Inflection point, at which the increasing evaporation trend with increasing precipitation reverses, shifts towards wetter scenarios for watersheds with higher hydraulic conductivity

Nine scenarios with same configuration as those used in the "Snow Dominant" case in Section 3.1, are repeated for six different equivalent watershed lateral hydraulic conductivity. The conductivities are obtained by multiplying the original watershed conductivity by a coefficient *Kh* equal to 1/10, 1/5, 1/2, 1, 2, 5 and 10. Even for a wide range of watershed conductivities, the general trend of WY evaporation that is observed in Section 3.1 persists. However, the magnitude of the WY evaporation increases with decreased watershed conductivity (Fig. 6). This is evident in the comparison of monthly variations in E_m and S_f for the two extreme conductivity cases with $Kh = 1/10$ and $Kh = 10$ (Fig. 7a–d). For $Kh = 1/10$, the average soil saturation in the watershed is larger, as the less conducting system is not efficient enough in transporting water out of the watershed. This results in a higher evaporation for a lower conductivity case. Notably, the difference in magnitude of evaporation between different *Kh* cases is smaller for greater WY precipitation. For increased WY precipitation scenarios, watershed averaged soil saturation is close to its maximum value of 1 during melt season and hence the difference in soil saturation between different conductivity cases is relatively small (Fig. 7a–d). This results in less sensitivity in the evaporation response to changes in watershed conductivity for the increased WY precipitation scenarios.

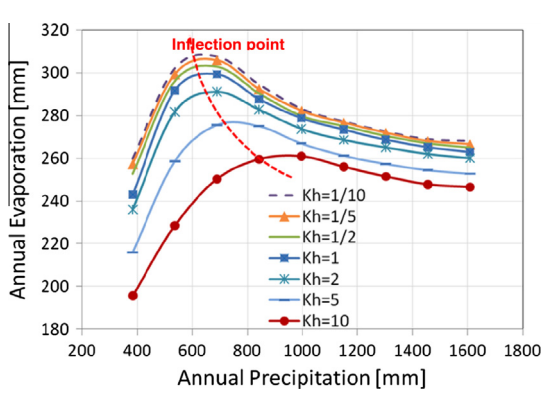

Fig. 6. Variation in evaporation with increasing amount of precipitation for a range of lateral hydraulic conductivities of the watershed. The conductivity of the watershed for different scenarios is equal to *Kh* times the original value.

Although conductivity modulation affects the magnitude of soil saturation, it does not significantly impact the rate of change in $S_{f,a}$ between different scenarios (Fig. 7f). At the same time, conductivity has negligible impact on the snow cover free period (Fig. 7f). Any marginal change in soil saturation due to a different watershed conductivity is expected to minimally affect the ground heat flux contribution to snow (an energy component which is generally small to begin with) and hence its affect on snow melt rate and $F_{f,a}$ is negligible. Since the rate of change of the two competing controls remain similar for different precipitation scenarios, the general trend of WY evaporation which initially increases and then subsequently decreases with increasing precipitation is still maintained for a wide range of hydraulic conductivity conditions (Figs. 6 and 7e).

However, the location of inflection point (where slope of the evaporation curve changes from increasing to decreasing) in WY evaporation trend is affected by the hydraulic conductivity of watershed (Figs. 6 and 7e). Low-conductivity watersheds exhibit an earlier inflection point than high-conductivity watersheds. For example, the inflection point of WY evaporation for $Kh = 1/10$ case is around WY precipitation of 600 mm while for $Kh = 10$, the inflection point is around WY precipitation of 900 mm (Fig. 6). This is due to greater average soil saturation for reduced conductivity cases. Since soil saturation is capped by its maximum value of 1 and soil saturation for less conducting cases is larger, the rate of increase in $S_{f,a}$ for reduced conductivity cases is also reduced (Fig. 7f). On the other hand, rate of increase in $S_{f,a}$ is greater for high-conductivity watersheds. As $F_{f,a}$ is not affected by the lateral conductivity, in the competition between the rate of increase in $S_{f,a}$ and the rate of decrease in $F_{f,a}$, the slope of $S_{f,a}$ dominates $F_{f,a}$ in the upper range of WY precipitation for high-conductivity watersheds than that for low-conductivity watersheds. This shifts the inflection point for high-conductivity watersheds toward larger WY precipitation scenarios (Fig. 7e).

3.3. Inflection point in the variation of evaporation with increasing WY precipitation shifts towards wetter scenarios for watersheds with smaller areal fraction of trees

Nine scenarios with the same designs as the ones used in the "Snow Dominant" case in Section 3.1, are repeated for three different vegetation configurations. The three configurations that are considered here include an in-situ vegetation distribution (Fig. 2) with 70% shrub (sagebrush) and 30% tree (hence forth referred as mixed case), an all shrub case and an all tree case. In this analysis, we consider all Aspen and Firs in tree class.

The results show that watershed averaged WY evaporation decreases with increase in the areal fraction of trees (Fig. 8). This is due to: (a) larger areal fraction of trees reduces soil evaporation by reducing net radiation to the ground, and (b) smaller net radiation also reduces the melt rate of snow thus prolonging snow cover duration and hence reducing soil evaporation even further. The anomalous trend (increasing and then decreasing) of WY evaporation with increasing WY precipitation, as shown in Section 3.1, still persists in all shrub and all tree cases. However, a larger tree-fraction in the watershed exhibits an earlier inflection point (Fig. 8). For a "tree dominant" watershed, reduction in net

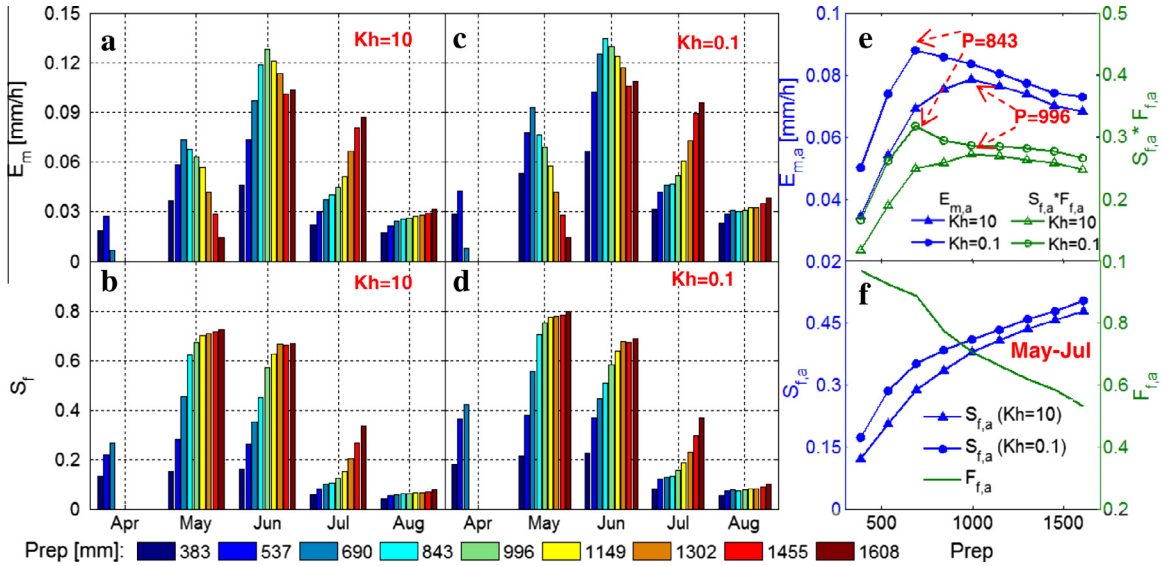

Fig. 7. Variations in monthly soil evaporation (E_m) and surface soil saturation during snow cover-free period (S_f) for different hydraulic conductivity conditions (Fig. 7a–d). The trends of $E_{m,a}$, $S_{f,a}$ and $F_{f,a}$ with increasing amount of WY precipitation are shown in Fig. 7e and f.

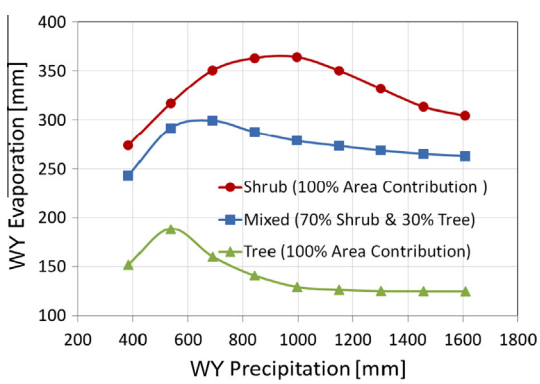

Fig. 8. Variation in evaporation with increasing amount of precipitation for different vegetation cover conditions.

radiation due to shading delays the melt of snow cover. This translates to persistent decrease in F_f with increase in WY precipitation (Fig. 9i). On the contrary, for a shrub dominant watershed, snow cover melts earlier during the year. In May–July, when meteorological variables such as net radiation and air temperature, that are primary controls on evaporation rates, have increased, a large proportion of the watershed surface is already snow-free (Fig. 9c). This translates to a reduction in the rate of decrease in $F_{f,a}$ (Fig. 9i). During the same period, the $S_{f,a}$ shows an increasing trend with increase in precipitation for both tree and shrub dominated setting. A sharper decrease in $F_{f,a}$ in tree dominant watershed results in shifting the inflection point toward reduced WY precipitation for "All Tree" case (Fig. 9g).

3.4. Inflection point in the variation of evaporation with increasing WY precipitation shifts towards wetter scenarios for watersheds with smaller areal fraction of snowfall

Hypsometry, location and watershed shape influences snowfall area fraction (SAF). Here we explore the impact of SAF on the trend of WY soil evaporation in relation to WY precipitation. Even though aerial coverage of precipitation in form of rain and snow in a watershed may vary from one event to other depending on meteorological conditions, here the analysis is presented for an average SAF during the water year. Four SAFs corresponding to 0%, 30%, 60% and 100% of the watershed area are considered in this experiment. Each SAF case includes nine precipitation scenarios. The temporal locations and magnitudes of precipitation events for each scenario are same as the ones used in Section 3.1. SAF of the watershed area is assumed to receive precipitation in form of snow, while the rest of the watershed is assumed to receive precipitation in form of rain. In this experiment, the watershed is assumed to be covered homogeneously by sagebrush. The configuration is considered so as to identify the sole effect of SAF on WY evaporation trends.

The WY soil evaporation increased SAF cases is reduced (Fig. 10). Larger SAF means less snow-free soil surface, thereby reducing soil evaporation. For example, for 0% SAF case, there is no snow cover shielding and hence F_f does not change with increasing WY precipitation. At the same time S_f increases with increasing WY precipitation resulting in monotonic increase in WY evaporation. With increased SAF, the variation in watershed averaged WY evaporation changes from a monotonically increasing to an increasing and subsequently decreasing trend. For 100% SAF case, F_f decreases with increasing WY snowfall, while S_f increases with increasing WY precipitation. So the competition between the rate of increase in $S_{f,a}$ and the rate of decrease in $F_{f,a}$ causes WY evaporation to first increase and then decrease with increasing WY precipitation. For intermediate SAF cases, the watershed averaged WY evaporation is the weighted sum of responses in the rain-fed and snow-fed areas. The relative fraction between the two determines the response of WY evaporation to WY precipitation. As the SAF increases from 0% to 100%, the inflection point for increasing SAF case shifts towards the smaller WY precipitation scenario (Fig. 10).

4. Conclusion

This paper explores the variation in soil evaporation vis-à-vis WY precipitation in the snow-dominated, semi-arid RME watershed. Different from the trend of WY evaporation characteristics of rain-dominated systems, where the WY evaporation increases monotonically with increasing precipitation, results show that WY evaporation initially increased and then subsequently decreased with increasing precipitation in a snow dominant setting. The expressed anomalous trend may have serious hydrologic

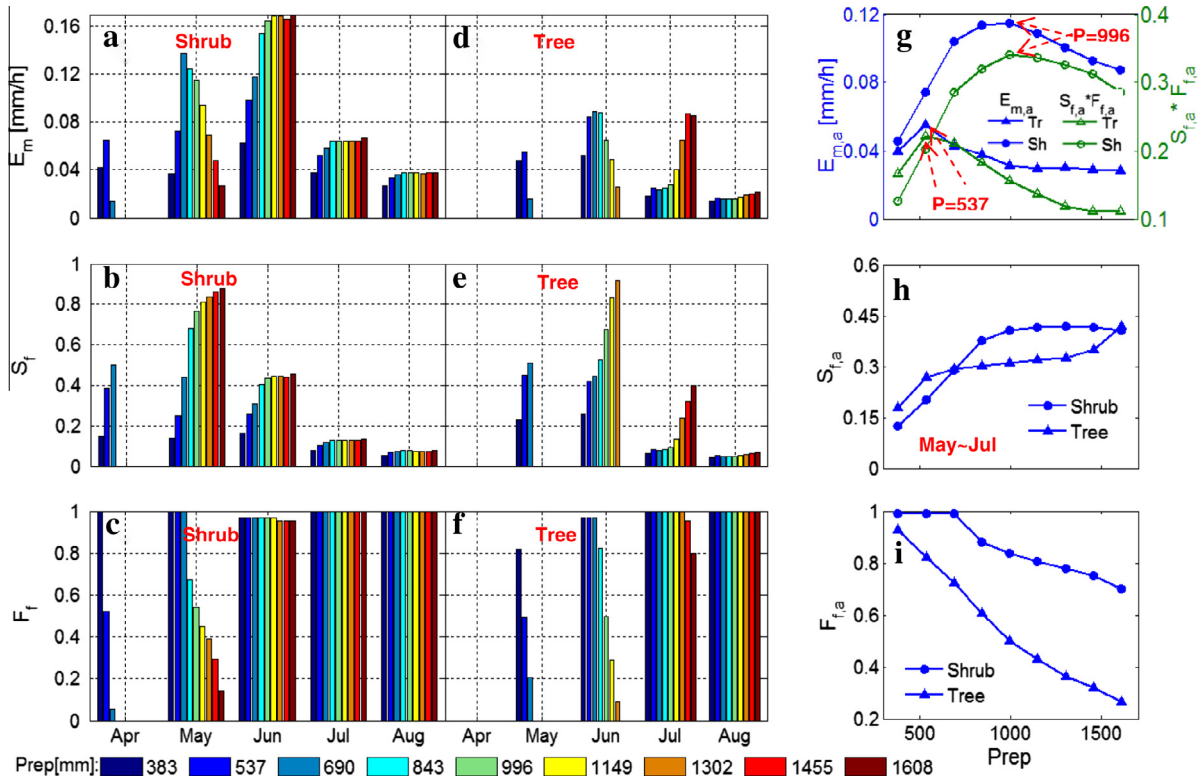

Fig. 9. Variation in monthly soil evaporation (E_m), surface soil saturation during snow cover-free period (S_f) and the fraction of snow cover-free period (F_f) for nine precipitation scenarios under "All Tree" and "All Shrub" vegetation cover cases (Fig. 9a–f). The tends of $E_{m,a}$, $S_{f,a}$ and $F_{f,a}$ with increasing amount of WY precipitation for "All Tree" and "All Shrub" cases are shown in Fig. 9g–i.

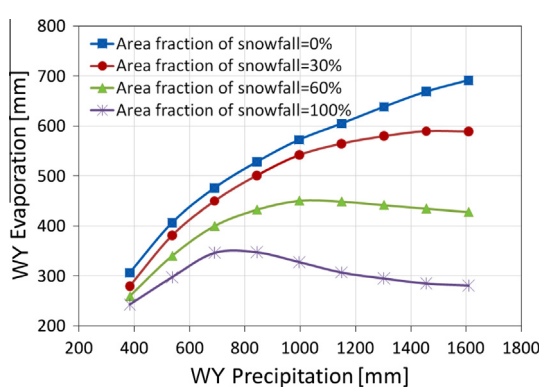

Fig. 10. Variation in WY evaporation with increasing WY precipitation for different area fraction of snowfall.

consequences, especially in sparsely vegetated watersheds where soil evaporation is a large fraction of total evapotranspirative flux. By comparing soil evaporation for rain and snow-dominated cases, it is further demonstrated that the trend is a unique characteristic of snow-dominated settings. The characteristic trend is identified to be due to a competition between the soil moisture available for evaporation and the duration of snow cover-free period. Generally, in snow-dominated semi-arid settings, an increase in precipitation contributes to more soil moisture available for soil evaporation, however it also increases snow cover period which negatively correlates to soil evaporation. Through a series of virtual experiments, we note that the anomalous trend persists across a wide range of conditions. While the analysis uses data from RME watershed, the simulated trends are expected to be prevalent in other snow-dominated watersheds, although with different intensity. Further experiments explore the effects of watershed characteristics such as hydraulic conductivity, relative fraction of shrubs and trees, and area fraction of snowfall on the soil evaporation trend. The results show that although the anomalous soil evaporation trend occurs across a wide range of watershed and meteorological conditions, the magnitude of the WY soil evaporation and location and timing of the inflection point in the trend changes. Watershed averaged WY evaporation is found to increase with a decrease in hydraulic conductivity of the watershed, areal fraction of trees vs. shrubs, and area fraction of snowfall. The inflection point of the trend shifts towards drier precipitation scenarios for cases with lower hydraulic conductivity, larger area fraction of trees and larger area fraction of snowfall. Meanwhile, transpiration exhibits an expected monotonic trend, in that it increases with increasing magnitude of precipitation. The rate of increase in transpiration is expected to be influenced by a number of factors including leaf area index, root zone depth, spatial distribution and depth of ground water table, and location of trees within the watershed. Based on the relative magnitudes of soil evaporation and transpiration, and their rates of variation with increasing precipitation, ET also shows an anomalous trend. However the rate of decrease in ET is much milder than that for soil evaporation. This research highlights the crucial role that snow cover duration plays in non-monotonic influence of snow accumulation and melt on WY evaporation and water budget. If validated, the results highlight the potential impacts on water availability in regards to variations in the magnitude and temporal distribution of precipitation in snow dominant watersheds.

Acknowledgements

This study was supported by the Duke University start-up grant for new faculties, and the data and analysis presented in this paper were funded in part by USDA-ARS CRIS Snow and Hydrologic

Processes in the Intermountain West (5362-13610-008-00D). Duke University and USDA are equal opportunity providers and employers. We thank Jeff Dozier and two other anonymous reviewers for constructive comments that greatly improved this paper.

Appendix A. Supplementary data

Supplementary data associated with this article can be found, in the online version, at http://dx.doi.org/10.1016/j.advwatres.2013.03.004.

References

[1] Itenfisu D, Ellion RL, Allen RG, Walter IA. Comparison of reference evapotranspiration calculations as part of the ASCE standardization effort. J Irrigat Drain Eng 2003;129:440–8. http://dx.doi.org/10.1061/(ASCE)0733-9437.
[2] Ramírez JA, Hobbins MT, Brown TC. Observational evidence of the complementary relationship in regional evaporation lends strong support for Bouchet's hypothesis. Geophys Res Lett 2005;32:L15401. http://dx.doi.org/10.1029/2005GL023549.
[3] Lundquist JD, Loheide II SP. How evaporative water losses vary between wet and dry water years as a function of elevation in the Sierra Nevada, California, and critical factors for modeling. Water Resour Res 2011;47:W00H09. http://dx.doi.org/10.1029/2010WR010050.
[4] Budyko MI. Climate and life. New York: Academic Press; 1974.
[5] Bandyopadhyay PK, Mallick S. Actual evapotranspiration and crop coefficient of wheat (Triticum aestivum L) under varying moisture levels of humid tropical canal command area. Agr Water Manage 2003;59:239–54. http://dx.doi.org/10.1016/S0378-3774(02)00112-9.
[6] Barnett TP, Adam JC, Lettenmaier DP. Potential impacts of a warming climate on water availability in snow-dominated regions. Nature 2005;438:303–9. http://dx.doi.org/10.1038/nature04141.
[7] Barnett TP, Pierce DW, Hidalgo HG, Bonfils C, Santer BD, Das1 T. Human-induced changes in the hydrology of the Western United States. Science 2008;319:1080–3. http://dx.doi.org/10.1126/science.1152538.
[8] Milly PCD, Dunne KA, Vecchia AV. Global pattern of trends in streamflow and water availability in a changing climate. Nature 2005;438:347–50. http://dx.doi.org/10.1038/nature04312.
[9] Kuhn TJ, Tate KW, Cao D, George MR. Juniper removal may not increase overall Klamath River Basin water yields. Calif Agr 2007;61:166–71.
[10] Flerchinger GN, Marks D, Reba ML, Yu Q, Seyfried MS. Surface fluxes and water balance of spatially varying vegetation within a small mountainous headwater catchment. Hydrol Earth Syst Sci 2010;14:965–78. http://dx.doi.org/10.5194/hess-14-965-2010.
[11] Flerchinger GN, Cooley KR. A ten-year water balance of a mountainous semi-arid watershed. J Hydrol 2000;237:86–99. http://dx.doi.org/10.1016/S0022-1694(00)00299-7.
[12] Kelleners TJ, Chandler DG, McNamara JP, Gribb MM, Seyfried MS. Modeling runoff generation in a small snow-dominated mountainous catchment. Vadose Zone J 2010;9:517–27. http://dx.doi.org/10.2136/vzj2009.0033.
[13] Shuttleworth WJ. Putting the 'vap' into evaporation. Hydrol Earth Syst Sci 2007;11:210–44. http://dx.doi.org/10.5194/hess-11-210-2007.
[14] Karamouze M, Zahraie B. Seasonal streamflow forecasting using snow budget and El Niño-Southern Oscillation climate signals: application to the Salt River Basin in Arizona. J Hydrol Eng 2004;9:523–33. http://dx.doi.org/10.1061/(ASCE)1084-0699(2004)9:6(523.
[15] Kim J, Miller, Guetter AK, Georgakakos KP. River flow response to precipitation and snow budget in California during the 1994/95 winter. J Climate 1998;11:2376–86. http://dx.doi.org/10.1175/1520-0442(1998)011<2376:RFRTPA>2.0.CO;2.
[16] Sridhar V, Nayak A. Implications of climate-driven variability and trends for the hydrologic assessment of the Reynolds Creek Experimental Watershed, Idaho. J Hydrol 2010;385:183–202. http://dx.doi.org/10.1016/j.jhydrol.2010.02.020.
[17] Kumar M, Marks D, Dozier J, Reba M, Winstral A. Evaluation of distributed hydrologic impacts of temperature-index and energy-based snow models. Adv Water Resour 2013. http://dx.doi.org/10.1016/j.advwatres.2013.03.006.
[18] McNamara JP, Chandler D, Seyfried M, Achet S. Soil moisture states, lateral flow, and streamflow generation in a semi-arid, snowmelt-driven catchment. Hydrol Process 2005;19:4023–38. http://dx.doi.org/10.1002/hyp.5869.
[19] Christensen L, Tague CL, Baron JS. Spatial patterns of simulated transpiration response to climate variability in a snow-dominated mountain ecosystem. Hydrol Process 2008;22:3576–88. http://dx.doi.org/10.1002/hyp.6961.
[20] Jeton AE, Dettinger MD, Smith JL. Potential effects of climate change on streamflow, eastern and western slopes of the Sierra Nevada, California and Nevada. US Geol Surv Water Resour Invest Rep 1996;95:4260.
[21] Reba M, Marks D, Seyfried M, Winstral A, Kumar M, Flerchinger G. A 25-year data set for hydrologic modeling in a snow-dominated mountain catchment. Water Resour Res 2011;47:W07702. http://dx.doi.org/10.1029/2010WR010030.
[22] Marks D, Winstral A, Seyfried M. Investigation of terrain and forest shelter effects on patterns of snow deposition, snowmelt and runoff over a semi-arid mountain catchment using simulated snow redistribution fields. Hydrol Process 2002;16:3605–26. http://dx.doi.org/10.1002/hyp.1237.
[23] Marks D, Kimball J, Tingey D, Link T. The sensitivity of snowmelt processes to climate conditions and forest cover during rain-on-snow: a case study of the 1996 Pacific Northwest flood. Hydrol Process 1998;12:1569–87. http://dx.doi.org/10.1002/(SICI)1099-1085(199808/09)12:10/11<1569::AID-HYP682>3.0.CO;2-L.
[24] Marks D, Domingo J, Susong D, Link T, Garen D. A spatially distributed energy balance snowmelt model for application in mountainous basins. Hydrol Process 1999;13:1935–59. http://dx.doi.org/10.1002/(SICI)1099-1085(199909)13:12/13<1935::AID-HYP868>3.0.CO;2-C.
[25] Qu Y, Duffy CJ. A semidiscrete finite volume formulation for multiprocess watershed simulation. Water Resour Res 2007;43:W08419. http://dx.doi.org/10.1029/2006WR005752.
[26] Kumar M. Toward a hydrologic modeling system. The Pennsylvania State University. ProQuest Dissertations and Theses, 274. http://search.proquest.com/docview/304984347?accountid=10598.
[27] Kumar M, Duffy CJ, Salvage KM. A second-order accurate, finite volume–based, integrated hydrologic modeling (FIHM) framework for simulation of surface and subsurface flow. Vadose Zone J 2009;8:873–90. http://dx.doi.org/10.2136/vzj2009.0014.
[28] Bhatt G, Kumar M, Duffy CJ. Bridging gap between geohydrologic data and Integrated Hydrologic Model: PIHMgis. Int Environ Model Software Soc (iEMSs) 2008.
[29] Allen RG, Pereira LS, Raes D, Smith M. Crop evapotranspiration: guidelines for computing crop water requirements-FAO irrigation and drainage paper 56; 1998.
[30] van Roosmalen L, Sonnenborg TO, Jensen KH. Impact of climate and land use change on the hydrology of a large-scale agricultural catchment. Water Resour Res 2009;45:W00A15. http://dx.doi.org/10.1029/2007WR006760.
[31] Krause P, Boyle DP, Bäse F. Comparison of different efficiency criteria for hydrological model assessment. Adv Geosci 2005;5:89–97. http://dx.doi.org/10.5194/adgeo-5-89-2005.